Gamma Ray Bursts and their afterglow properties

Poonam Chandra[1][*] and Dale A. Frail[2]

[1]*Department of Physics, Royal Military College of Canada, Kingston, ON K7M3C9, Canada*
[2]*National Radio Astronomy Observatory, 1003 Lopezville Road, Socorro, NM 87801, USA*

Abstract. In this paper, we review the afterglow properties of 304 Gamma Ray Bursts observed with various radio telescopes between the year 1997 to January 2011. Most of the observations in the sample presented here were performed in the 8.5 GHz band with the Very Large Array. Our sample shows that the detection rate for the radio afterglows has stayed at about 31% for the pre-*Swift* as well as the post-*Swift* bursts, in contrast to large increases in the optical and X-ray afterglow detection rates. Our detailed analysis of the detected versus the non-detected radio afterglows shows that these are severely limited by the instrument sensitivity. We also find that there is no obvious correlation between the radio luminosity with the isotropic γ-ray energy release, the γ-ray fluence, or with the X-ray flux; however, the optical afterglows fluxes show a weak correlation with the radio flux density. Radio afterglow detection is dependent upon a relatively narrow range of circumburst densities (1–10 cm^{-3}) and microscopic shock parameters, especially the magnetic energy density. Finally we discuss the most interesting bursts and some of the interesting current topics in the GRB field.

1. Introduction

Gamma Ray Bursts (GRBs) were discovered serendipitously in 1967 and reported in 1973 (Klebesadel, Strong & Olson 1973). They are the brightest explosions in the Universe after the Big Bang. The isotropic energies emitted by GRBs range from $10^{51} - 10^{54}$ erg, released in just a few seconds. In a standard framework of *relativistic fireball model* of GRBs (Rees & Meszaros 1992; Sari, Piran & Narayan 1998), the explosion results in an ejection of material at ultrarelativistic speeds and even though a GRB lasts only from a fraction of a second (short GRBs) to several seconds (long GRBs), the relativistic ejecta moving into the surrounding circumburst medium

---

[*]email: Poonam.Chandra@rmc.ca

creates a forward shock emitting in the lower wavebands lasting from several days (in X-rays) to months (in radio), called the afterglow emission.

Our understanding of GRBs has advanced rapidly since the discovery of the long-lived "afterglows" at X-ray, optical and radio wavelengths (Costa et al. 1997; van Paradijs et al. 1997; Wijers, Rees & Meszaros 1997; Frail et al. 1997a). The earlier searches for radio afterglow emission were strongly motivated by theoretical arguments that predicted a time-variable radio source at the mJy level days or weeks following a GRB (Paczynski & Rhoads 1993; Katz 1994). However, searches for radio afterglow emission (Frail et al. 1994), as well as for the prompt radio emission (Dessenne et al. 1996) remained unsuccessful. The main reason for this lack of success was likely due to the crude GRB localizations (roughly a few degrees) provided by existing instruments. To image these large fields of view, searches had to be carried out at low frequencies (less than a few GHz) where the radio afterglow flux density is greatly reduced by synchrotron self-absorption (when the absorption of the radiation by the synchrotron electron themselves becomes important). The launch of the BeppoSAX satellite revolutionized GRB astronomy by rapidly (hours) disseminating accurate (arcminutes) GRB positions. The first radio counterpart was detected 30 years after the first GRB (Frail et al. 1997a). Since that time many more $\gamma-$ray and hard X-ray satellites have monitored the sky for GRBs providing accurate localizations and enabling detailed follow up by the space and ground-based facilities at longer wavelengths. As a result this large and sustained effort, several hundred afterglows have been detected over the last 15 years. This work has exposed a rich diversity of GRB behaviours and several distinct progenitor classes (Gehrels, Ramirez-Ruiz & Fox 2009).

In the 15 years, since the first radio afterglow discovery from GRB 970508, radio studies of GRB afterglows have become an integral part of GRB physics. Unlike optical or X-ray wavelengths, radio observations present the possibility of following the full evolution of the fireball emission through all of its different stages; first, synchrotron self absorbed light curve while it is optically thick, then as it slowly rises to a peak flux density and thereafter decays, making a transition from an ultrarelativistic to subrelativistic shock. Synchrotron self-absorption, interstellar scintillation, forward shocks, reverse shocks, jet-breaks, non-relativistic transitions and obscured star formation are among the phenomena routinely observed through radio observations. The scintillation of the radio source (Goodman 1997) and its flux density in the optically thick epoch, when it is synchrotron self-absorbed (Katz 1994), allow a determination of the size and expansion of the fireball (e.g. GRB 970508). Radio observations are now routinely used in broadband modelling of afterglows and uniquely probe the density structure of the circumburst medium (Harrison et al. 2001; Panaitescu & Kumar 2001; Yost et al. 2003; Chandra et al. 2008; Cenko et al. 2011). Radio studies have also proven useful for inferring the opening angles of the jetlike outflows, since its observational signature differs from that at optical and X-ray wavelengths (Harrison et al. 1999; Berger et al. 2000, 2001; Frail et al. 2000a). Short-lived radio flares, most likely due to reverse shock, have also been detected from radio observations (Kulkarni et al. 1999; Berger et al. 2003b; Nakar & Piran 2005; Chandra et al. 2010) and seems more common in radio bands than in the optical bands. The radio afterglow, due to its long-lived nature, explores the time when the jet expansion has become subrelativistic and quasi-spherical (Frail et al. 2000b, 2005; van der Horst et al. 2008), and determines calorimetry of the burst. An exclusive property of radio

afterglow is their detection even at high redshifts (Frail et al. 2006; Chandra et al. 2010) due to the negative *k*-correction effect (Ciardi & Loeb 2000). Thus radio afterglow studies provide unique diagnostics on GRB explosions, their progenitors, and their environments.

While many of the early advances were made by studying individual GRBs and their afterglows, now much more can be learned from the study of large samples (Sakamoto et al. 2008, 2011). Compilations of X-ray and optical light curves from the *Swift* satellite have revealed complex but canonical light curve behaviours (Nousek et al. 2006; Evans et al. 2007; Melandri et al. 2008; Roming et al. 2009; Evans et al. 2009). Optical catalogues have derived mean dust extinction laws of GRB host galaxies (Kann, Klose & Zeh 2006; Starling et al. 2007), and have led to claims of clustering of the optical afterglow luminosities (Liang & Zhang 2006). The standard fireball model has been tested through spectral and temporal comparisons of X-ray and optical light curves (e.g. Oates et al. 2009, 2011). Significant differences have been found between the mean brightness and the redshift distribution of *Swift* and pre-*Swift* GRBs (Berger et al. 2005; Jakobsson et al. 2006; Kann et al. 2010). Correlations have been found for both short- and long-duration bursts between the gamma-ray fluence and the X-ray and optical afterglow brightness (Gehrels et al. 2008; Nysewander, Fruchter & Pe'er 2009). A population of dark bursts, which has no or very faint optical emission, has been identified (Rol et al. 2005), as has a population of nearby, low luminosity events (Kann et al. 2010).

In comparison, very little effort has gone into compiling radio afterglow data and carrying out correlative studies (Berger 2004). A catalogue of the first five years of radio afterglow data was produced by Frail et al. (2003), but comparisons were limited just between detection rates of X-ray, optical and radio afterglows. The mean flux densities and luminosities of radio afterglows were given in Frail (2005), while Soderberg et al. (2006) compiled radio light curves to compare GRB and supernova luminosities. Since the launch of the *Swift* satellite the number of GRBs with radio data has doubled. Moreover, in the near future the continuum sensitivity of the Very Large Array[1] (VLA) - the primary telescope for radio afterglow follow-up – will increase by a factor of 5 to 20 (depending on wavelength). In Chandra & Frail (2011) we pull together all the past radio data in one place and to use the catalogue to define the average properties of radio afterglows, search for trends in different sub-classes of bursts and investigate various correlations. Here we reiterate the major results from Chandra & Frail (2011) and present an extensive review of a radio selected sample of GRBs and their afterglow properties. We also identify the interesting problems where the future of GRB afterglow studies should concentrate on.

In §2, we present a summary of our radio sample and its properties. We compare the detection statistics with respect to other wave bands. We also discuss the details and statistics of detection versus upper limits of our sample. Correlative properties with other waveband parameters are discussed in §2.5. We produce synthetic model light curves of GRB afterglows and discuss their dependence on various parameters in §3. Some of the most interesting bursts are discussed in §4 and current hot topics are discussed in §5. We discuss our findings in §6.

---

[1]The Very Large Array is operated by the National Radio Astronomy Observatory, a facility of the National Science Foundation operated under cooperative agreement by Associated Universities, Inc.

Throughout the paper, we adopt a Λ-CDM cosmology with $H_0 = 71$ km s^{-1} Mpc^{-1}, $\Omega_m = 0.27$ and $\Omega_\Lambda = 0.73$ (Spergel et al. 2007).

2.   Radio afterglows of Gamma Ray Bursts

This section is mainly a summery of our paper Chandra & Frail (2011). We reproduce the main figures from Chandra & Frail (2011) and discuss them in context of this paper.

Our compiled sample consists of 304 GRBs observed with the radio telescopes between 1997 to 2011. This sample includes 35 Short-hard bursts (SHBs), 19 X-ray flashes (XRFs) and 25 GRBs with possible supernova associations (SN/GRBs). The SN/GRB category in this paper includes all the GRBs with confirmed supernova associations as well as possible associations (see Hjorth & Bloom 2011). The sample also includes one candidate galactic transient (GRB 070610, Kasliwal et al. 2008).

A total of 270 afterglows were observed as part of the VLA radio afterglow programs, and 15 bursts were observed by the Expanded VLA (EVLA), whereas Australia Telescope Compact Array (ATCA) was used to look at 19 southern bursts. Among the total of 285 VLA/EVLA bursts, 8 bursts were followed by the ATCA, 38 bursts were observed by the Westerbork Synthesis Radio Telescope (WSRT), 19 VLA/EVLA bursts were followed by the Ryle telescope, and 11 bursts were observed by the Giant Metrewave Radio Telescope (GMRT). The Very Long Baseline Array (VLBA) with its sub-milliarcsecond angular resolution was used to observe five bursts of the VLA/EVLA bursts (please refer to Table 4 of Chandra & Frail (2011) for a list of all the radio telescopes used to observe an individual burst). For the VLA observations, most of the afterglows were observed in the 8.5 GHz frequency band. The detected GRBs were followed up with observations in other wavebands. Most of the WSRT observations were carried out in 5 GHz band, Ryle telescope observations in 15 GHz band and the GMRT observations in 1420 MHz band.

2.1   Multiwaveband detection statistics of our sample

A total of 95 out of 304 bursts were detected in radio bands, resulting in a detection rate of 31%. In Fig. 1, we plot the histogram of annual number of GRBs radio afterglow searches and the number of successful detections. A large increase in the radio afterglow observations is seen soon after the launch of *Swift*.

We subdivide the sample into pre-*Swift* (total of 123 bursts) and post-*Swift* bursts (a total of 181 bursts) to investigate any possible selection biases. In Fig. 2, we plot the Venn diagram for our entire sample as well as for pre-*Swift* and post-*Swift* sample illustrating the different relationships between the radio, optical and X-ray observations of the afterglows. We exclude all those bursts which were either not observed in any of the bands, or not detected in all bands, as well as those events which had an unconfirmed detection in any of the bands. Finally we included a total of
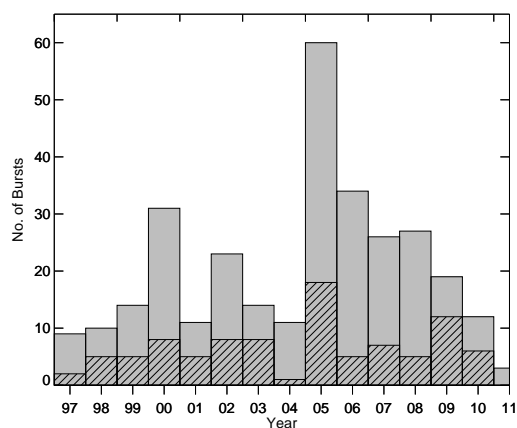
Figure 1. Histogram of the annual number of GRB afterglow searches (filled histogram) and the number of successful detections (hatched histogram). There are a total of 304 searches and 95 detections.
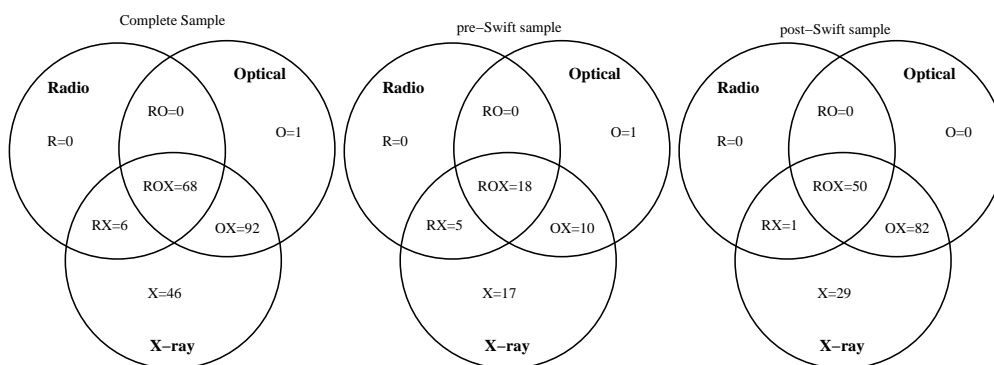

Figure 2. Venn diagram illustrating the different relationships between the radio, optical, and X-ray afterglows (Chandra & Frail 2011). The symbols X, O and R indicate detections in X-ray, optical and radio bands respectively. RX indicates detection in radio and X-ray but not in optical, while ROX indicates afterglows seen in all three bands.

213 bursts. In Fig. 2, X-ray detections are marked with X, optical detections are marked with O and radio detections are marked with R. ROX indicates the bursts which were detected in all three bands, whereas a combination of two letters indicates a joint detection in the respective bands.

Our sample consists of 68 bursts which were detected in all three bands. In pre-*Swift* sample, the GRBs detected in all three bands was only 18, rising to 50 in the post-*Swift* bursts. The radio detection statistics in pre-*Swift* and post-*Swift* samples essentially remained unchanged i.e. 42/123 (34%) in pre-*Swift* and 53/181 (29%) in post-*Swift*. In contrast, the X-ray detection rates increase from 41% to 93% after the launch of *Swift*. The optical detection rates also increased

Table 1. K–M estimates of the flux density distribution.

Freq. GHz (1)	Time range Days (2)	Total Detections (3)	Total Data points (4)	KM$_{25}$[a] μJy (5)	KM$_{50}$[b] μJy (6)	KM$_{75}$[c] μJy (7)	Mean flux μJy (8)
4.86	2 − 8	27	63	243	155	64	197 ± 17
4.86	5 − 10	17	40	238	88	44	193 ± 23
4.86	7 − 14	20	39	237	132	82	206 ± 27
8.46	2 − 8	65	157	199	107	31	162 ± 15
8.46	5 − 10	51	107	196	92	55	170 ± 20
8.46	7 − 14	43	99	185	92	26	173 ± 22

Notes: (a) K–M estimates that 25% of all bursts will have radio afterglows above this value; (b) K–M estimates that 50% of all bursts will have radio afterglows above this value; (c) K–M estimates that 75% of all bursts will have radio afterglows above this value.

from 47% to 75% between pre-*Swift* and post-*Swift* bursts. This is attributed to the on-board X-ray telescope (XRT) and UV/optical telescope (UVOT) which were autonomously slewed to the burst position, and also due to the availability of rapid, well-localized positions for ground-based follow-up.

2.2 Radio flux density distributions and upper limits

Since our data consists of upper limits as well as detections, we incorporated Kaplan–Meier Product Limit method (K–M; Feigelson & Nelson 1985) in making estimates of the flux density distributions. The K–M estimator was applied to a sample of bursts for which flux density measurements had been made at one frequency over a fixed time interval. For detections, we averaged multiple observations of the same GRB over the desired time range, since over the short periods the flux density variations at radio frequencies are dominated by interstellar scintillation. Table 1 summarizes our results for 5 and 8.5 GHz bands. Here, we tabulate the frequency and the time range for which the data were used. The mean estimates take into account the detections as well as the upper limits. The 3rd and 4th columns in the table lists the number of detections and total number of data points, respectively. The 5th, 6th and 7th columns tabulate the estimates of minimum flux density, above which 25%, 50%, and 75 % of the total radio afterglows will lie. Column 7 lists the K–M estimates of the mean flux densities including detections and upper limits.

Before making any detailed comparisons, it is important to understand any possible biases that might exist in these data. Specifically, we ask whether a radio non-detection is the result of an inadequate measurement (i.e., not observing at a correct time or with enough sensitivity), or whether it is the result of an underlying physical cause. In Fig. 3, we plot all the radio upper limits
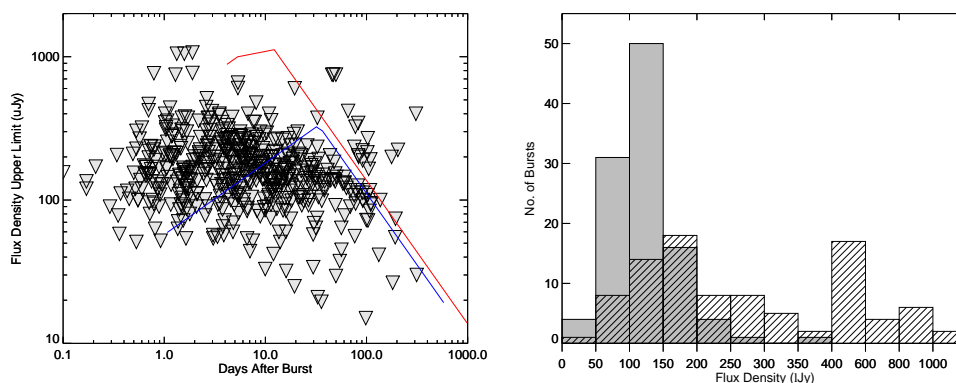
Figure 3. **Left:** Upper limits at 5 and 8.5 GHz frequency band for all GRBs for which no afterglow was detected (Chandra & Frail 2011). The red, upper line represents the light curve of a bright event GRB 980703 and the blue, lower line represents the light curve of a more typical event GRB 980329. The detection fraction of radio afterglows appears to be mainly limited by sensitivity, at least for the first 10 days. **Right:** Gray filled histogram represents the flux density distribution for upper limits at 8.5 GHz frequency band for GRBs in our sample between days 5–10. The hatched histogram shows the flux density distribution for the detections between days 5–10.

at 8.5 GHz obtained using K–M method, overlay with detected light curves of one bright GRB light curve GRB 980703 (red, upper curve) and a more typical GRB 980329 (blue, lower curve). The plot shows that our upper limits do not cut off at a fixed flux density but are tightly clustered within one order of magnitude (between 30 μJy to around 400 μJy). As illustrated in Fig. 3, most of the observations would be capable of detecting a bright GRB 980703-like afterglow, while up to the first 10 days (when most of the afterglow observations take place), only around 50% observations would have been capable of detecting an average event like GRB 980329. This result suggests that radio afterglow searches are strongly sensitivity limited. Here, we also plot the histogram distribution of radio upper limits as well as the detections between 5–10 days. The upper limits peak in 100–150 μJy range, whereas the detections peak in 150–200 μJy range. As first noted by Frail (2005), the difference in the upper limits and the detections is not highly significant. There is only about a factor of 50 difference between the radio flux density of the brightest and the faintest detected cosmological bursts (i.e. z >0.4). This low dynamic range stands in sharp contrast to the orders of magnitude difference between the bright and faint events seen in either X-ray or afterglow samples (Kann, Klose & Zeh 2006; Racusin et al. 2011). This narrow flux density range reinforces our suggestion that the detection fraction of our radio afterglow sample is determined by instrumental sensitivities.

2.3 Canonical light curves of radio afterglows

In Fig. 4, we plot all the light curves of detected radio afterglows at 8.5 GHz in the rest frame and the observer frame for cosmological long bursts ($z \geq 0.4$, Chandra & Frail 2011). We average
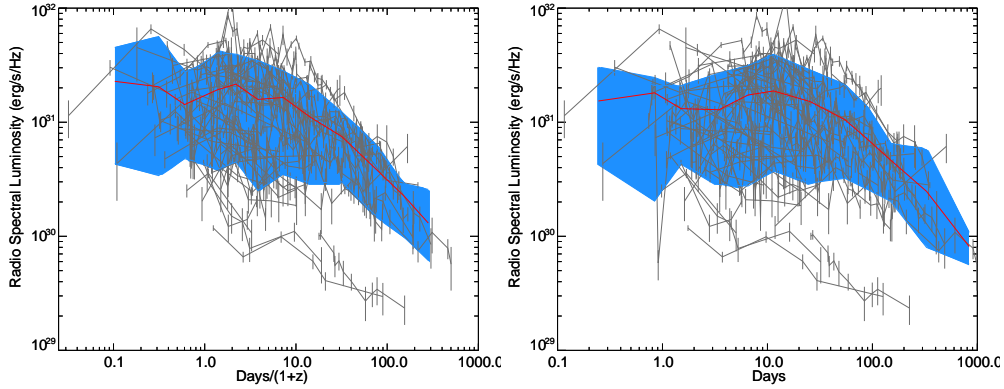
Figure 4. Individual and mean radio light curves at 8.5 GHz band for the long-duration, cosmological GRBs in the rest frame time (Chandra & Frail 2011). The red solid line represents the mean light curve. The blue area represents the 75% confidence band. The right panel shows the same plot for time in the observer's frame.

these data to produce a mean light curve for long-duration, cosmological GRBs (LGRB) as a red line along with 75% confidence bands (blue area). A canonical LGRB if observed from beginning to end will have a mean luminosity of $\sim 2 \times 10^{31}$ erg/s/Hz until about 3-6 d (10-20 d) in the rest-frame (observer-frame). After this time there is a gradual power-law decay with an index of order -1. The mean light curve shows two peaks (rest frame), one between day 0.1–0.2 and one around day 2, and a dip around day 1. The first peak is not significant since there are too few data points. The peak after day 2 is likely to be significant. The dip near day 1 appears real and may signify a transition between two different emission components i.e. forward shock and reverse shock.

In Fig. 5, we plot the radio luminosity light curves for the different GRB classes at 8.5 GHz band. The top left plot is the light curve for short-hard bursts (SHBs), whose time duration is usually less than 2 seconds (Kouveliotou et al. 1993). Our sample included 35 SHBs but there are only two detections GRB 050724 and GRB 051221A. We also overlay the mean light curve of the long cosmological GRBs (LGRBs). It is clear that SHBs are intrinsically radio dim objects. They are more than an order of magnitude fainter than a LGRB. In the upper right frame of Fig. 5 we plot the light curves of the 19 X-ray flashes (XRFs) in our sample which includes seven detections. Most XRFS are usually only about a factor of ten fainter than LGRB (red curve). The extreme outlier is GRB 060218, which is 4-5 orders of magnitude dimmer than a typical event. In the lower frame of Fig. 5 we selected only those 9 GRBs for which the known SN associations is exist. The SNe/GRBs nearly fully populate this radio luminosity plot. Some SNe/GRBs such as GRB 980425 and GRB 060218 are dim, while others like GRB 030329 are as bright as a typical LGRB. SHBs are intrinsically the dimmest and shortest lived explosions. XRFs and SN/GRBs are comparable in their radio luminosity but they are still about an order of magnitude fainter, on average, compared to LGRBs.
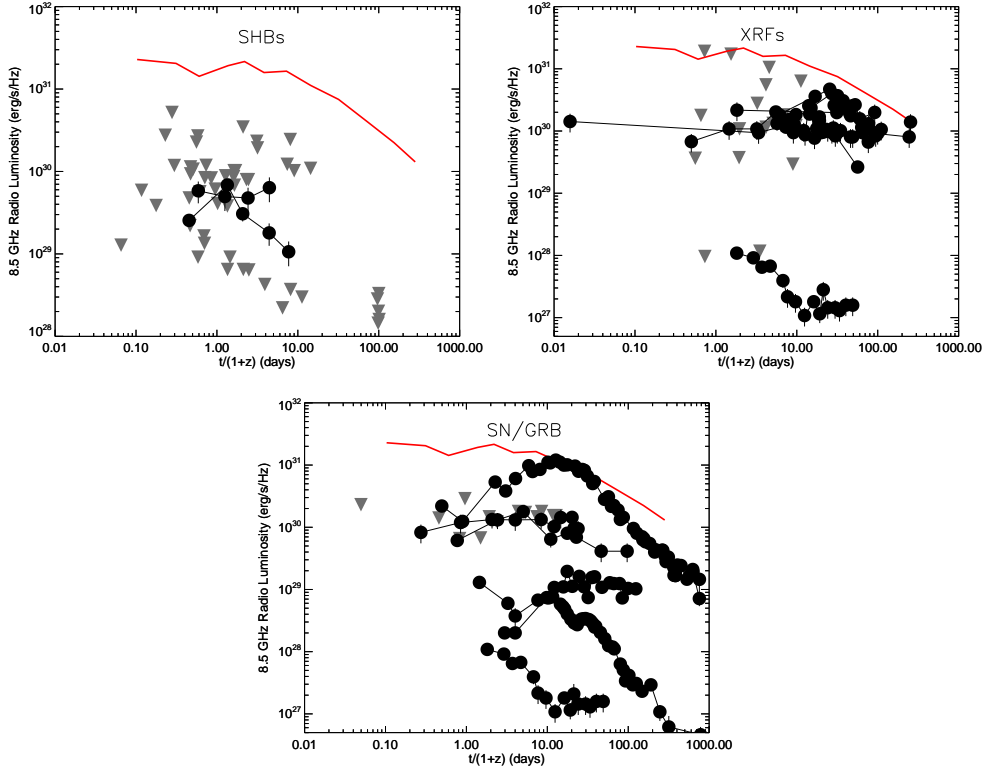
Figure 5. A compilation of radio luminosity curves in the rest frame for three different populations of GRBs: short hard bursts (top left), X-ray flashes (top right), and supernova-GRB associations (bottom). The red solid line represents the mean light curve for the long-duration, cosmological sample. The figure is taken from (Chandra & Frail 2011).

2.4 Peak flux density and redshift distributions

For the detected radio afterglows with radio light curves (i.e. 3 or more detections in one single radio band), we determined the peak flux density and the time at the peak flux density using Eq. 1 of Chandra & Frail (2011). We note that most of the radio afterglows peak between $3 - 6$ days in the rest frame (Chandra & Frail 2011). This could be due to the ν_m passing the radio frequencies around this time. Another possibility is that jet breaks in GRBs occur mostly around this time and radio stops rising after the occurrence of jet break. The peak luminosity distribution at 8.5 GHz band indicates that the luminosities peak between $10^{31} - 10^{32}$ erg/s/Hz.

In our radio-selected sample of 304 GRBs, we have 147 GRBs with known redshifts. We have 100 GRBs with redshift available in post-*Swift* epoch as compared to just 47 bursts with known

redshifts in pre-*Swift* epoch. GRB 090423 is the object with highest confirmed spectroscopic redshift of $z = 8.26$, whereas the highest photometric redshift in our sample ($z = 9.4$) is for GRB 090429B. GRB 980425 is the object with lowest redshift with $z = 0.0085$. The average redshift of our sample is $\langle z \rangle = 1.78$. The average redshifts in pre- and post-*Swift* bursts are $\langle z \rangle^{pre} = 1.34$ and $\langle z \rangle^{post} = 1.99$, respectively (Chandra & Frail 2011). The mean redshift for the pre-*Swift* bursts is similar to the value $\langle z \rangle = 1.4$ derived by Jakobsson et al. (2006), though they measure $\langle z \rangle = 2.8$ for a post-*Swift* optically-selected sample. Instrumental sensitivity may explain the origin of this bias in our radio-selected sample to slightly lower redshifts for post-*Swift*. As first noted by Ciardi & Loeb (2000) and shown by Frail et al. (2006), the detection rate of radio afterglows is largely insensitive to redshift (negative *k*-correction effect). However, despite this effect the mean peak flux density at $z \sim 2.8$ is close to the sensitivity limit of existing instruments where it is increasingly difficult to detect radio afterglows reliably.

2.5   Correlative properties

Here we investigate whether radio afterglow strength depends upon the gamma-ray burst properties (fluence, duration, isotropic and beaming-corrected energy) and the X-ray and optical afterglow properties. Here we estimate the correlation between the radio afterglow and the above properties in terms of Pearson's correlation coefficient, or *R*-index. We chose only cosmological long GRBs to investigate the correlative properties.

We did not see any correlation between the radio afterglow versus fluence, duration or isotropic energy. We also do not see any correlation between peak radio afterglow with the X-ray flux at 1/2 day (when the X-ray emission strength becomes independent of the density (Nysewander, Fruchter & Pe'er 2009)). The only positive correlation we see is between the optical flux at R-band at 11hr and the corresponding peak radio flux density. The beaming angle and jet break time also show positive correlations with the radio afterglow emission. However, since only 46 GRBs in our sample had observed jet breaks (or limits on the jet break times), this correlation may be biased and a larger sample is required to check the true correlation for the jet break time and the beaming angle with the radio brightness of the afterglows.

3.   Synthetic radio light curves

In this section, we plot synthetic light curves of GRB radio afterglows to determine their dependence on various environmental parameters as well as on microscopic parameters. In Fig. 6, synthetic light curves of GRBs are plotted at various frequencies. Here we fix a redshift $z = 3$ and density $n = 10 \, \mathrm{cm}^{-3}$. We also fix other parameters such as, isotropic kinetic energy $E_{KE,iso} = 10^{53}$ erg, beaming angle $\theta_j = 0.2$ rad, relativistic energy fraction $\epsilon_e = 0.1$, magnetic energy fraction $\epsilon_B = 1\%$, and electron spectral index $p = 2.2$. The canonical GRB parameters that we use here are good averages from the afterglow broadband modelling (Panaitescu & Kumar 2001; Yost et al. 2003). We note that the 1.4 GHz flux density is suppressed at all times (due to large absorption). The figure indicates that while the lower frequencies peak at later times (as expected), they
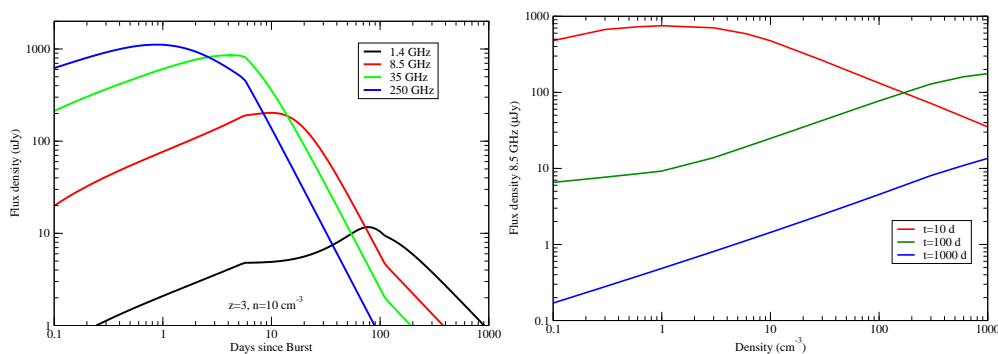
Figure 6. Left panel: Plot of radio flux density light curves at various frequencies for a redshift of 3 and density of 10 cm^{-3}. Right panel: Density dependence of radio afterglow at 8.5 GHz and $z = 1$ for various days.

have lower peak flux densities as well. ALMA 250 GHz and EVLA 35 GHz bands are the two best bands to detect radio afterglows. Previous 250 GHz mm bands of various telescopes and the 35 GHz VLA bands were not sensitive enough to detect weak radio afterglows. In the right panel, we plot the radio flux density as a function of circumburst density at various days. The other parameters are fixed as above. This shows that even the bright bursts in high density may be faint early on, but will become radio bright if observed at late times. In a low-density medium, early-on observations give the brightest radio emission. For $t = 10$ d, the afterglow is brightest in a unity density medium.

We now plot the radio afterglow flux density dependence on various parameters. We again fix the parameters as indicated above (see Fig. 7). The plots are made for typical EVLA band at 8.5 GHz at redshift of 3 and 8, respectively. The radio afterglow is a strong function of density as indicated. The strength of radio afterglow depends upon two competing effects: increase in flux density due to enhanced synchrotron emission in high density and decreased flux density due to increase in synchrotron self absorption effects (internal absorption by the medium) in high density. The figure shows that the radio afterglow is brightest for densities between $n = 1 - 10$ cm^{-3}. At lower densities, the afterglow is intrinsically weak, whereas at higher densities, synchrotron self absorption effects are suppressing the radio afterglow strength for a long duration. This may also explain why some of the bright GRBs are dim in radio band. If observed at very late epochs, we may see an increase in flux density. Radio emission is also a sensitive function of the magnetic energy density. We note that higher the magnetic energy density, brighter the radio afterglow is. This is not surprising since the synchrotron emission is more efficient in the presence of a high magnetic field. However, plots of radio lightcurves versus relativistic electron energies are very weakly dependent on the electron energy density. This may explain as to why some of the bright bursts with high isotropic energies are not radio bright. If less amount of energy goes in magnetic field and more energy goes to electrons, radio emission will not be strong enough to be detectable.
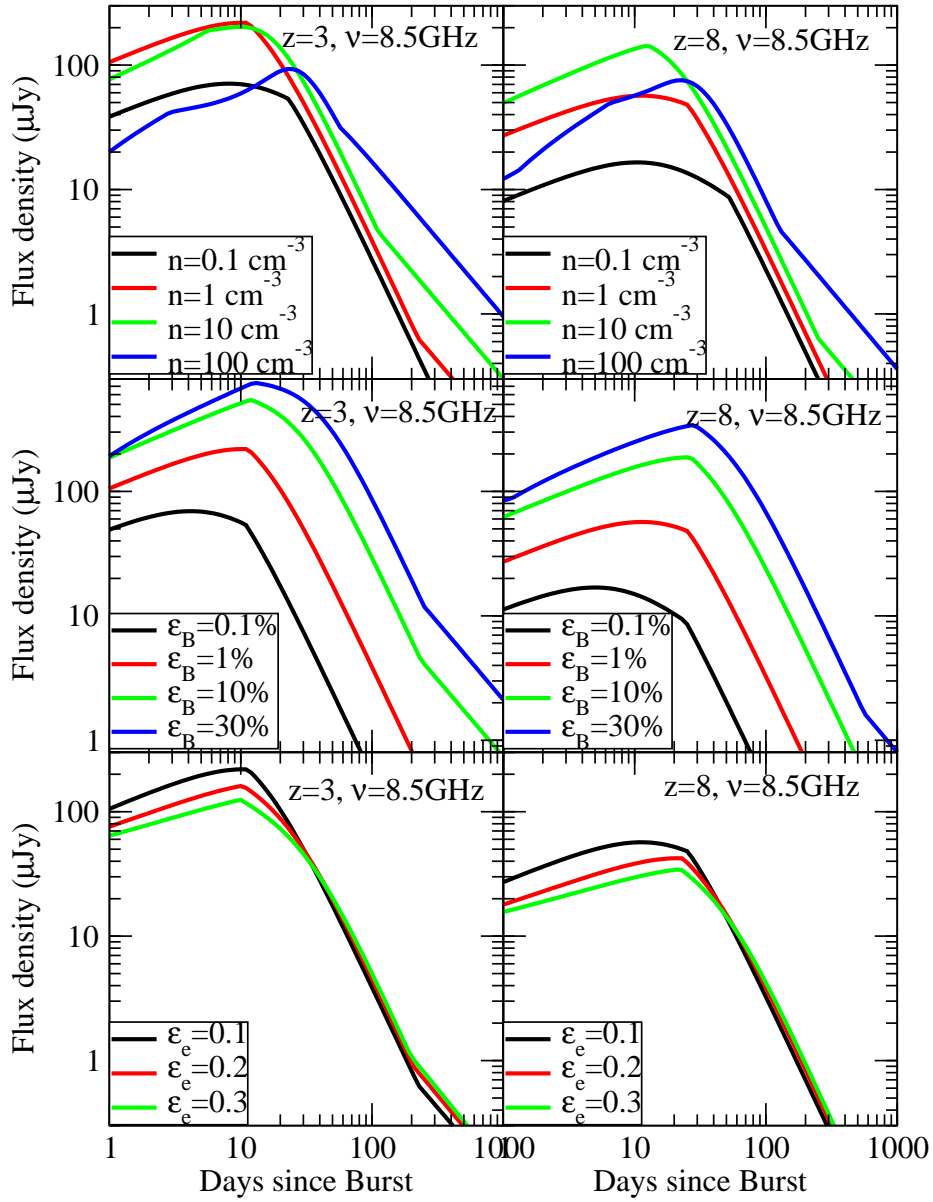
Figure 7. Plot of radio flux density light curves as a function of density n, magnetic energy density ϵ_B and electron energy density ϵ_e. We have shown the dependence at $z = 3$ (plots in left panel) and for $z = 8$ (plots in right panel).

4.   Bursts of special interest

In this section, we describe some radio afterglows of great interest, which made a great impact and contribution in shaping the GRB afterglow field.

GRB 970508 was the first GRB from which a radio afterglow emission was discovered (Frail et al. 1997a), owing to the precise localization of the GRB with the BeppoSAX. The optical spectroscopy of GRB 970508 clearly demonstrated the cosmological origin of the burst, resolving a long-standing controversy about the distance scale to GRBs. The initial radio flux density fluctuations were interpreted as interstellar scintillations, which lead to an estimation of the fireball size (Frail et al. 1997a,b; Waxman, Kulkarni & Frail 1998). They deduced the size of the burst to be about 3 microarcseconds. Synchrotron self absorption effect lead to an independent size measurement (Katz & Piran 1997), consistent with the one obtained from the scintillation. This also demonstrated superluminal expansion and provided an early confirmation of the fireball model. GRB 970508 remained bright more than a year after the discovery, when the ejecta had reached sub-relativistic speeds making the energetics independent of geometry of the burst. This gave the most accurate estimate of the kinetic energy of the burst ($E_{KE} = 0.5 \times 10^{51}$ erg (Frail et al. 2000b)).

GRB 990123 was the first burst from which a radio emission was clearly detected 1 day after the burst, after which it rapidly faded away. This was in contrast to other bursts, which rise to peak flux density on a timescale of a week and then decay over several weeks to months. This radio flare on day 1 was interpreted as an emission from the reverse shock (Kulkarni et al. 1999). The relative faintness of the observed late-time radio emission also provided an independent indication of a jetlike geometry in this GRB. The clear evidence of reverse-shock in radio band suggested that the radio flare phenomenon has the potential to shed new light on the physics of reverse shocks in GRBs.

GRB 030329 at a redshift of $z = 1.6$ was the first cosmological burst with a clear supernova association (Price et al. 2003). This was the first spectroscopic evidence of a GRB supernova association confirming the massive star origin of GRBs. Very Large Baseline Interferometry (VLBI) of GRB 030329 provided direct measurement of the GRB size and expansion speeds (Taylor et al. 2004; Pihlström et al. 2007). This established the most direct evidence of relativistic motion of the fireball in a GRB explosion.

GRB 070125 was one of the brightest *Swift* GRB which remained radio bright for more than a year (Chandra et al. 2008). The interstellar scintillation put tight upper limits on the fireball size. The afterglow modelling demonstrated that the burst resided in a high density medium. This GRB demonstrated a case of chromatic jet break, with X-ray jet break appearing at a later time than the optical jet break. Inverse Compton effects provided the most comprehensive explanation of the delay in jet break in the X-ray bands.

GRB 090423 at a redshift of 8.3 is the highest redshift known object in the Universe (Tanvir et al. 2009). The GRB was detected in radio bands for several tens of days (Chandra et al. 2010).

The multiwaveband modelling indicated the unity density medium and the massive star origin of the GRB, confirming that star formation was taking place even at a redshift of 8.3. The properties of the GRB, though, was not sufficient enough to distinguish between the population II versus a Population III kind of progenitor of the GRB.

5. Current hot topics in GRB radio afterglows

5.1 Lack of jet breaks

Since *Swift* launch, as the data in X-ray and optical bands is far better sampled, there has been a dearth of measurements of jet opening angles (Panaitescu 2007; Kocevski & Butler 2008; Liang et al. 2008; Racusin et al. 2009). Most strikingly, surprisingly few *Swift* afterglows have shown the characteristic achromatic steepening associated with a collimated outflow. Several groups have conducted a comprehensive analysis of a large sample of X-ray (Panaitescu 2007; Kocevski & Butler 2008; Racusin et al. 2009) and/or optical (Liang et al. 2008) light curves, finding that at most only a small fraction exhibit clear evidence for collimation. Without these collimation corrections, the true energy release from *Swift* events has remained highly uncertain. The most natural explanation for this discrepancy can be attributed to the high sensitivity of *Swift*, because of which the *Swift* is preferentially selecting GRBs with smaller isotropic γ-ray energies, $E_{\gamma,iso}$, values compared with pre-*Swift* missions. The result is that *Swift* jet breaks are expected to occur on average later than those of pre-*Swift* events, making jet-break measurements quite difficult (Perna, Sari & Frail 2003). Given the typical follow-up capabilities of a medium-aperture telescope, jet breaks are virtually undetectable for a majority of Swift GRBs (Kocevski & Butler 2008).

However, there have been some cases, where chromatic jet breaks are also seen (Chandra et al. 2008). For example, in GRB 070125, the X-ray jet break occurred at a later time than the optical jet break and the cause of chromaticity was attributed to the effective inverse Compton (IC) effect, which have no effect on the low energies, but shifting the X-ray jet break at a later time (Chandra et al. 2008). Radio observations are an important indicator of the effectiveness of the IC effect, as they dominate only in high density environment and radio is the unique frequency to probe the density of the medium. Chandra et al. (2008) showed that for a given density of GRB 070125, the estimated delay in X-ray jet break due to the IC effect is consistent with the observed delay. This area needs to be explored further for other GRBs.

5.2 Hyperenergetic events

In the standard model of a long duration GRB, a compact central engine is responsible for accelerating and collimating the jet-like outflows. The precise nature of the central engine remains an open question. However, empirical constraints require all long duration GRBs to have the kinetic energies of order 10^{51} erg. Estimations of collimated corrected energy of GRBs suggested

that the beaming corrected energy was indeed tightly clustered around 10^{51} erg (Frail et al. 2001; Berger et al. 2003a; Bloom, Frail & Kulkarni 2003). However, since that time it is becoming increasingly evident that the actual range of relativistic energy may be much wider. A population of nearby subluminous GRBs have relativistic energy lease many orders of magnitude smaller than a typical GRB (Soderberg et al. 2004). More recently, evidence has been growing for a class of GRBs whose total relativistic energy release is at least an order of magnitude above the canonical value of 10^{51} erg (such as GRBs 050820A, 050904, 070125, 080319B, 090323, 090423, 090926A, Chandra et al. 2008, 2010; Chandra & Frail 2011; Cenko et al. 2010, 2011). The total energy budget of these hyper-energetic events poses a significant challenge for some progenitor models. This suggests that GRBs are perhaps a more diverse population than originally thought.

However, the estimates on energy in *Swift* era have larger uncertainties. This is attributed to the fact that the limited bandpass of *Swift*-BAT captures only a small fraction of the total $\gamma-$ray energy, and can entirely miss the peak of the $\gamma-$ray spectrum. Thus measuring bolometric fluences (in $1 - 10^4$ keV range) of *Swift* events has proven to be a challenging task. Lack of observed jet breaks also causes huge uncertainty in the beaming corrected energy estimation. With its huge energy coverage (10 keV-100 GeV), *Fermi* can provide unparalleled constraints on the spectral properties of the prompt emission and can distinguish between the true hyper-energetic bursts (such as GRB 090323, 090902B, 090926A, Cenko et al. 2011). However, *Fermi* is sensitive to GRBs with very large isotropic energy releases (10^{54} erg), which are rare events (although important for testing the central engine models). An additional concern, motivated by the double-jet models for GRB 030329 (Berger et al. 2003b; van der Horst et al. 2005) and GRB 080319B (Racusin et al. 2008), is our assumption that the entire relativistic outflow is collimated into a uniform jet with a single opening angle. It would ease the sometimes extreme efficiency requirements if the $\gamma-$ray emission were more narrowly beamed than the afterglow.

Late time radio afterglow observations, when the flow has become subrelativistic offer a unique insight into the energy problem. At late stages, the jet would have expanded sideways so much that it would essentially become quasi-spherical and independent of the jet geometry, giving handle of the accurate calorimetry of GRBs. However, this is possible only for GRBs with bright radio afterglows. Alternatively, higher sensitivity radio telescopes can observe the afterglow for a longer time and provide the accurate energy estimation. The Atacama Large Millimeter Array (ALMA) also has a important role to play since GRB spectrum at early times peak at mm wavelengths, when it is brightest. ALMA with its high sensitivity can detect such events and give better estimation of the kinetic energy of the burst.

5.3   High redshift bursts

Understanding the reionization of the Universe, when the first luminous sources were formed, is one of the latest frontiers of observational cosmology. Constraints have been obtained using diagnostics such as quasar studies of the Gunn-Peterson absorption trough, the luminosity evolution of Ly$-\alpha$ galaxies, and the polarization isotropy of the cosmic microwave background. Taken together, these data portray a complicated picture in which reionization has taken place over a

range of redshifts rather than at one specific epoch. The dominant source of reionization appears to be due to ultraviolet emission from young, massive stars (see review by Fan, Carilli & Keating 2006).

As the most luminous explosions in the Universe, GRBs are detectable out to large distances, and due to their connection to core-collapse supernovae, they are the potential signposts of these early massive stars. They could in principal reveal the stars that form from the first dark matter halos ($z \sim 20 - 30$) through the epoch of reionization at $z = 11 \pm 3$ and closer (Lamb & Reichart 2000; Ciardi & Loeb 2000; Gou et al. 2004). The radio, infrared, and X-ray afterglow emission from GRBs are in principle observable out to $z \sim 30$ (Miralda-Escude 1998; Lamb & Reichart 2000; Ciardi & Loeb 2000; Gou et al. 2004; Ioka & Mészáros 2005). Thus GRB afterglows make ideal backlights to probe the intergalactic medium as well as the interstellar medium in their host galaxies. Predicted to occur at redshifts beyond those where quasars are expected, they could be used to study both the reionization history and the metal enrichment of the early Universe (Totani et al. 2006). The fraction of detectable GRBs that lie at high redshift ($z > 6$) is, however, expected to be less than 10% (Perley et al. 2009; Bromm & Loeb 2006).

So far there are only 3 GRBs with confirmed measured redshifts z>6: GRB 050904 (Kawai et al. 2006), GRB 080913 (Greiner et al. 2009) and GRB 090423 (Tanvir et al. 2009) with $z = 6.3$, $z = 6.7$, and $z = 8.3$, respectively. Just the mere discovery of all three bursts have confirmed that massive stellar formation occurred in the very early Universe. Radio flux density show only a weak dependence on the flux, due to the "negative *k*-correction" effect (Ciardi & Loeb 2000). In this effect, the afterglow flux density remains high because of the dual effects of spectral and temporal redshift, offsetting the dimming due to the increase in distance (Lamb & Reichart 2000). Even though GRB 080913 was never detected in radio (only 30% bursts are detected in radio bands at high redshifts), but GRB 050904 and GRB 090423 were detected in radio bands at various epochs. Radio observations of these bursts allowed us to put constraints on the density of the GRB environments at such high redshifts. While the density of GRB 090423 was of the order of unity (perfectly capable of hosting a Pop III progenitor GRB explosion), the density of GRB 050904 was 2 orders of magnitude higher, indicating dense molecular cloud surrounding the GRB. Thus the two GRBs exploded in a very different environments.

Both GRBs, 050904 and 090423, show possible reverse shock signatures in their early radio observations. The mm band is ideal to look for reverse shock signatures at high redshifts, as the effects of time dilation almost compensate for frequency redshift, resulting in a near-constant observed peak frequency in the mm band ($\nu \sim 200$ GHz) at a few hours post-event, and a flux density at this frequency that is almost independent of redshift (Inoue, Omukai & Ciardi 2007). ALMA, with its high sensitivity (~ 75 μJy in 4 minutes), will be a potential tool for selecting potential high-*z* bursts that would be high priority for intense follow-up across the spectrum. This will hopefully greatly increase the rate at which high-*z* events are identified. With an order of magnitude enhanced sensitivity the EVLA will be the perfect instrument to study a high-*z* GRB for a longer timescale. For a 2 hr integration in the 8 GHz band, the EVLA can reach sensitivity up to 2.3 μJy which will be able to detect the GRB 090423-like burst for almost 2 years. EVLA will thus be able to detect fainter events and follow events like GRB 050904 and GRB 090423

for a longer duration, therefore obtaining better density measurements, better estimates of outflow geometry, and the total kinetic energy.

6.   Discussion and conclusions

In this paper we discuss a radio-selected sample of 304 GRBs based on 15 years of observations. In addition to the radio observations, we have collected supplementary data including redshift, gamma-ray fluence, and optical and X-ray flux densities on all bursts (Chandra & Frail 2011, and references therein). Previous studies (e.g. Gehrels et al. 2008; Nysewander, Fruchter & Pe'er 2009; Kann et al. 2010) have not included radio data in the analysis.

We show that the fractional detection rate of radio afterglows is 31% (§2.1). These detection statistics do not change substantially between the pre-*Swift* (42/123 or 34%) and post-*Swift* (53/181 or 29%) samples. This is markedly different than the factor of two increase in the detection probability of optical and X-ray afterglows post-*Swift*, mainly attributed to *Swift*'s on-board detection, autonomous slews, and the availability of rapid, well-localized positions, which are not realized by the slower evolving radio afterglows.

Next we investigated the flux density distribution of the radio afterglows for cosmological GRBs (§2.2). We have used a Kaplan–Meier estimator to estimate the realistic mean flux density estimates. We also showed that range between peak flux density of the brightest afterglow and the faintest afterglow spans only a narrow range (a factor of fifty), in sharp contrast to optical and X-ray afterglows which range over several orders of magnitude limit. Together this suggests that the radio afterglow searches are strongly sensitivity limited.

We investigated the luminosity distribution of several sub-classes of GRBs including the long-duration, cosmological GRBs (LGRB), short-hard bursts (SHB), X-ray flashes (XRF) and GRBs with firm supernova associations (SNe/GRB). There are a wide spread of luminosities for these different subclasses with long GRBs (LGRBs) the brightest on average, while SHBs are nearly two orders of magnitude fainter than LGRBs, and XRFs and SNe/GRBs are ten times fainter than LGRBs, albeit with a large scatter. The best sampled radio light curves is that of the LGRB class with multiple data points that range from nearly 0.01 d to 1000 d. The canonical LGRB will reach a peak luminosity of $\sim 2 \times 10^{31}$ erg/s/Hz about 3 to 6 days in the rest frame, and after about 10 to 20 days will undergo a power law decline with an index of order unity (§2.3). There is some (not strong) evidence of two equally luminous emission components with a transition occurring at 1 d in the rest frame. The early component may be the result of the reverse shock as has been claimed previously for several bursts (Kulkarni et al. 1999; Fox et al. 2003; Berger et al. 2003b; Chandra et al. 2010) while the later component is the standard forward shock which has been studied through extensive broad-band modelling (Wijers & Galama 1999; Panaitescu & Kumar 2001; Yost et al. 2003).

Correlations were explored between the radio flux density and gamma-ray fluence, optical flux density and X-ray flux density. Additionally, we also explored the correlations between the

radio and the jet break time and beaming angle. There are only 3 significant correlations in our sample, these are correlations between peak radio and optical flux at 11hr, peak beaming-corrected radio luminosity with jet break time as well as with beaming angle. However, the data points are very small for the correlations involving peak beaming-corrected radio luminosity because of jet breaks known only in a very limited cases.

The synthetic light curves §3 indicate that radio afterglow emission will be brightest for densities between $n = 1 - 10$ cm^{-3}. In the range outside this, the flux density will be weak either due to a low intrinsic emission strength (lower densities) or due to synchrotron self absorption suppression (higher densities). The radio afterglow strength strongly depends upon the scheme of equipartition energy distribution, with bias towards magnetic energy density.

Acknowledgements

References

Berger E. et al., 2000, ApJ, 545, 56
Berger E. et al., 2001, ApJ, 556, 556
Berger E. et al., 2003a, ApJ, 590, 379
Berger E., Soderberg A. M., Frail D. A., Kulkarni S. R., 2003b, ApJ, 587, L5
Berger E., 2004, Astronomical Society of the Pacific Conference Series, 312, 163
Berger E. et al., 2005, ApJ, 634, 501
Bloom J. S., Frail D. A., Kulkarni S. R., 2003, ApJ, 594, 674
Bromm V., Loeb A., 2006, ApJ, 642, 382
Cenko S. B. et al., 2010, ApJ, 711, 641
Cenko S. B. et al., 2011, ApJ, 732, 29
Chandra P. et al., 2008, ApJ, 683, 924
Chandra P. et al., 2010, ApJ, 712, L31
Chandra P., Frail D. A., 2011, submitted to ApJ
Ciardi B., Loeb A., 2000, ApJ, 540, 687
Costa E. et al., 1997, Nature, 387, 783
Dessenne C. A.-C. et al., 1996, MNRAS, 281, 977
Evans P. A. et al., 2007, A&A, 469, 379
Evans P. A. et al., 2009, MNRAS, 397, 1177

Fan X., Carilli C. L., Keating B., 2006, ARA&A, 44, 415

Feigelson E. D., Nelson P. I., 1985, ApJ, 293, 192

Fox D. W. et al., 2003, ApJ, 586, L5

Frail D. A. et al., 1994, ApJ, 437, L43

Frail D. A. et al., 1997a, Nature, 389, 261

Frail D. A. et al., 1997b, ApJ, 483, L91

Frail D. A. et al., 2000a, ApJ, 534, 559

Frail D. A., Waxman E., Kulkarni S. R., 2000b, ApJ, 537, 191

Frail D. A. et al., 2001, ApJ, 562, L55

Frail D. A., Kulkarni S. R., Berger E., Wieringa M. H., 2003, AJ, 125, 2299

Frail D. A., 2005, in Marcaide J. M., Weiler K. W., eds., IAU Colloq. 192: Cosmic Explosions,
    On the 10th Anniversary of SN1993J, Berlin: Springer, p. 451

Frail D. A. et al., 2005, ApJ, 619, 994

Frail D. A. et al., 2006, ApJ, 646, L99

Gehrels N. et al., 2008, ApJ, 689, 1161

Gehrels N., Ramirez-Ruiz E., Fox D. B., 2009, ARA&A, 47, 567

Goodman J., 1997, New Arrivals, 2, 449

Gou L. J., Mészáros P., Abel T., Zhang, B., 2004, ApJ, 604, 508

Greiner J. et al. 2009, ApJ, 693, 1610

Harrison F. A. et al., 1999, ApJ, 523, L121

Harrison F. A. et al., 2001, ApJ, 559, 123

Hjorth J., Bloom J. S., 2011, arXiv:1104.2274

Inoue S., Omukai K., Ciardi B., 2007, MNRAS, 380, 1715

Ioka K., Mészáros P., 2005, ApJ, 619, 684

Jakobsson P. et al., 2006, A&A, 447, 897

Kann D. A., Klose S., Zeh A., 2006, ApJ, 641, 993

Kann D. A. et al., 2010, ApJ, 720, 1513

Kasliwal M. M. et al., 2008, ApJ, 678, 1127

Katz J. I., 1994, ApJ, 432, L107

Katz J. I., Piran T., 1997, ApJ, 490, 772

Kawai N. et al., 2006, Nature, 440, 184

Klebesadel R. W., Strong I. B., Olson R. A., 1973, ApJ, 182, L85

Kocevski D., Butler N., 2008, ApJ, 680, 531

Kouveliotou C. et al., 1993, ApJ, 413, L101

Kulkarni S. R. et al., 1999, ApJ, 522, L97

Lamb D. Q., Reichart D. E., 2000, ApJ, 536, 1

Liang E., Zhang, B., 2006, ApJ, 638, L67

Liang E.-W., Racusin J. L., Zhang B., Zhang B.-B., Burrows D. N., 2008, ApJ, 675, 528

Melandri A. et al., 2008, ApJ, 686, 1209

Miralda-Escude J., 1998, ApJ, 501, 15

Nakar E., Piran T., 2005, ApJ, 619, L147

Nousek J. A. et al., 2006, ApJ, 642, 389

Nysewander M., Fruchter A. S., Pe'er A., 2009, ApJ, 701, 824

Oates S. R. et al., 2009, MNRAS, 395, 490

Oates S. R. et al., 2011, MNRAS, 412, 561

Paczynski B., Rhoads J. E., 1993, ApJ, 418, L5

Panaitescu A., 2007, MNRAS, 380, 374

Panaitescu A., Kumar P., 2001, ApJ, 560, L49

Perley D. A. et al., 2009, AJ, 138, 1690

Perna R., Sari R., Frail D. A., 2003, ApJ, 594, 379

Pihlström Y. M., Taylor G. B., Granot J., Doeleman S., 2007, ApJ, 664, 411

Price P. A. et al., 2003, Naure, 423, 844.

Racusin J. L. et al., 2008, Nature, 455, 183

Racusin J. L. et al., 2009, ApJ, 698, 43

Racusin J. L. et al., 2011, arXiv:1106.2469

Rees M. J., Meszaros P., 1992, MNRAS, 258, 41

Rol E., Wijers R. A. M. J., Kouveliotou C., Kaper L., Kaneko Y., 2005, ApJ, 624, 868

Roming P. W. A. et al., 2009, ApJ, 690, 163

Sakamoto T. et al., 2008, ApJS, 175, 179

Sakamoto T. et al., 2011, ApJS, 195, 2

Sari R., Piran T., Narayan R., 1998, ApJ, 497, L17

Soderberg A. M. et al., 2004, Nature, 430, 648

Soderberg A. M. et al., 2006, Nature, 442, 1014

Spergel D. N. et al., 2007, ApJS, 170, 377

Starling R. L. C. et al., 2007, ApJ, 661, 787

Tanvir N. R. et al. 2009, Nature, 461, 1254

Taylor G. B., Frail D. A., Berger E., Kulkarni S. R., 2004, ApJ, 609, L1

Totani T. et al., 2006, PASJ, 58, 48

van der Horst A. J. et al., 2005, ApJ, 634, 1166

van der Horst A. J. et al., 2008, A&A, 480, 35

van Paradijs J. et al., 1997, Nature, 386, 686

Waxman E., Kulkarni S. R., Frail D. A., 1998, ApJ, 497, 288

Wijers R. A. M. J., Galama T. J., 1999, ApJ, 523, 177

Wijers R. A. M. J., Rees M. J., Meszaros P., 1997, MNRAS, 288, L51

Yost S. A., Harrison F. A., Sari R., Frail D. A., 2003, ApJ, 597, 459